

Recent Experiments Assessing the Uncertainty of Metal Cutting Temperature Measurements When Using the NIST High-Speed Dual-Spectrum Optical System

Eric Whittenton^a, April Cooke^a, Jarred Heigel^b, and Ivan Arriola Aldamiz^c

^aNational Institute of Standards and Technology, Gaithersburg MD, USA, 20899

^bKT Consulting Inc., Antioch, CA, USA, 94509

^cMondragon University, Loramedi 4, 20500 Mondragon, Guipuzcoa, Spain

ABSTRACT

Process models, including finite element modeling simulations, are important for optimizing the metal cutting process, allowing industry to make parts faster, better, and at less cost. Measurements of the process can be used to improve and verify the accuracy of these models. There are many error sources when using infrared radiation thermography to measure the temperature distribution of the tool, workpiece, and chip during metal cutting. Furthermore, metal cutting presents unique measurement challenges due to factors such as the high magnification required, high surface speeds, micro-blackbody effects, and changing emissivity as chips form.

As part of an ongoing effort to improve our understanding of uncertainties associated with these thermographic measurements, two sets of experiments were performed. One set explored how well the surface temperature of the cutting tool accurately reflects the internal temperature. This was accomplished by simultaneously measuring the temperature using both a thermal camera and a thermocouple embedded within the cutting tool.

The other set investigated correcting for motion blur, point spread function, and a less than ideal range of sensitivity of the thermal camera when measuring the shear zone temperature of the chip. In theory, this correction could be performed using deconvolution. Unfortunately, deconvolutions are sensitive to noise and it is difficult to gauge the uncertainty of the computed values. Thus, convolutions of various assumed inputs were computed and compared to the measured temperatures. Assumed inputs which yielded a good fit to the measured temperatures were considered candidate values. The range of those candidate values yields a measure of the uncertainty of the calculation.

Keywords: uncertainty, metal cutting, dual-spectrum, high-speed imaging, infrared thermography

INTRODUCTION

1.1 Conventions

In general, the first time an important concept is discussed in this paper it is presented in ***bold italic*** while variable names are presented in *italic*. ***True temperature*** refers to the actual temperature of an object. ***Apparent temperature*** refers to the temperature a “perfect” camera measures, and includes properties of the scene being imaged such as emissivity and reflections. Note that this is not necessarily the same as the ***imaged temperature***, which is the temperature the camera actually reports, and also includes properties of the image acquisition process such as scattering in the camera optics. The symbol \cong means “corresponding to.”

Disclaimer: This document is an official contribution of the National Institute of Standards and Technology and is not subject to copyright in the United States. The National Institute of Standards and Technology does not recommend or endorse commercial equipment or materials, nor does it imply that the equipment or materials shown are necessarily the best available for the purpose.

1.2 Why measure metal cutting temperatures?

Modeling is an important tool for optimizing the metal cutting process, allowing industry to make parts faster, better, and at less cost⁽¹⁾. Measurements of the process using thermal^(2; 3) and visible^(4; 5) imaging can be used to improve and verify the accuracy of these models. Four goals of manufacturing-related research at the National Institute of Standards and Technology (NIST) are; develop and improve measurement techniques, develop an understanding of the uncertainties involved with performing such measurements, compare models of machining to thermal and visible spectrum images to verify the models, and to share this understanding with the machining community.

Figure 1 shows a schematic of a typical image of an orthogonal cutting process. The relative motion between a **cutting tool** and a **workpiece** causes material to be removed from the workpiece. This removed material is referred to as a **chip**. Most of the deformation of the workpiece material occurs within a thin area called the **shear zone**.

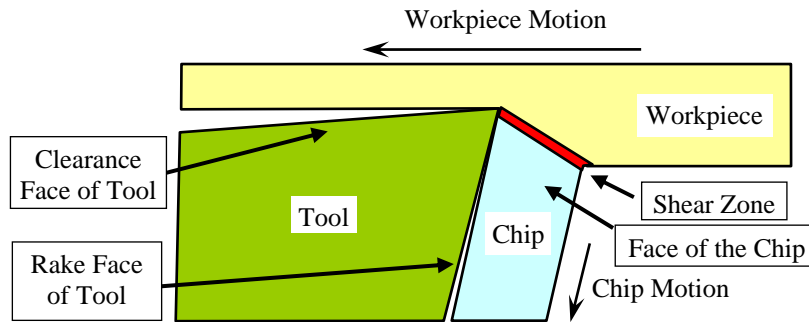


Fig. 1. Schematic of an image of an orthogonal cutting process.

Two of the many types of chips are called continuous and segmented. A **continuous chip** is a long ribbon of relatively uniformly deformed material. By contrast, a **segmented chip** has alternating zones of low and high shear strain. A zone of low strain in a segmented chip is called a **segment**. The zones of high strain between the segments are mechanically weak, so the long ribbons of material tend to break into short pieces. These short pieces are more manageable than a continuous chip. Even when segmented chips do not break completely, there is generally a partial gap between the segments. The shear zone is somewhat stationary when continuous chips are formed, but often travel along with the chips when the chips are segmented. We will call the area surrounding the shear zone the **face** of the chip. The shear zone has a higher temperature than the face. For segmented chips, the shear zone generally also has a higher emissivity than the face.

1.3 The high-speed dual-spectrum system.

The custom built high-speed dual-spectrum system typically images the side of the tool, workpiece, and chip as the chip is being formed. There is a range of camera settings used, depending on the cutting conditions and the aspect of machining being investigated. Other dual-spectrum systems have recently appeared in the literature⁽⁶⁾. It should be noted that the cutting conditions and materials studied at NIST are industrially relevant. If a parameter, such as surface speed, is too fast and causes the images to be inaccurate, NIST works to either improve the imaging system or learn how to answer research questions using images which are attainable. Early work by some researchers used very slow cutting. This makes for high quality images of cutting conditions which, unfortunately, are of limited value to industry.

Generally, the images obtained with the high-speed dual-spectrum system have about a 1 mm by 1 mm field of view. The visible spectrum images are typically acquired at 30 000 frames per second, yielding 256 pixel by 128 pixel images. The workpiece and chip are typically traveling between 0.5 m/s and 5 m/s. To maximize image sharpness, the integration time is adjusted to the shortest possible while still producing acceptable images. The thermal spectrum images are typically acquired at 160 pixel by 120 pixel, 300 frames per second, from 3.8 μm to 5.1 μm in wavelength. Where practical, integration time is adjusted to maximize image sharpness while maintaining enough sensitivity to image temperatures of interest.

Figure 2 shows the NIST customized camera system. The main lens is a reflective lens that passes both visible and infrared light. The cold mirror reflects visible light to the visible light camera and transmits infrared light to the thermal camera. Temperature controlled water is circulated to stabilize the temperatures of the optics. Through-the-lens lighting aids positioning of the camera system by projecting a spot of visible light onto the object being imaged. At an angle to the dual-spectrum system is a conventional camcorder which images the scene at a low magnification. A data acquisition system records the timing of the thermal and visible spectrum images, along with analog data such as cutting forces. Custom software allows all of the data streams to be played back in a synchronized manner. Figure 3 shows a typical data set. In this example, the true temperature at a given location in the tool as a function of time is computed. Such a rich data set facilitates many aspects of machining research⁽⁷⁾.

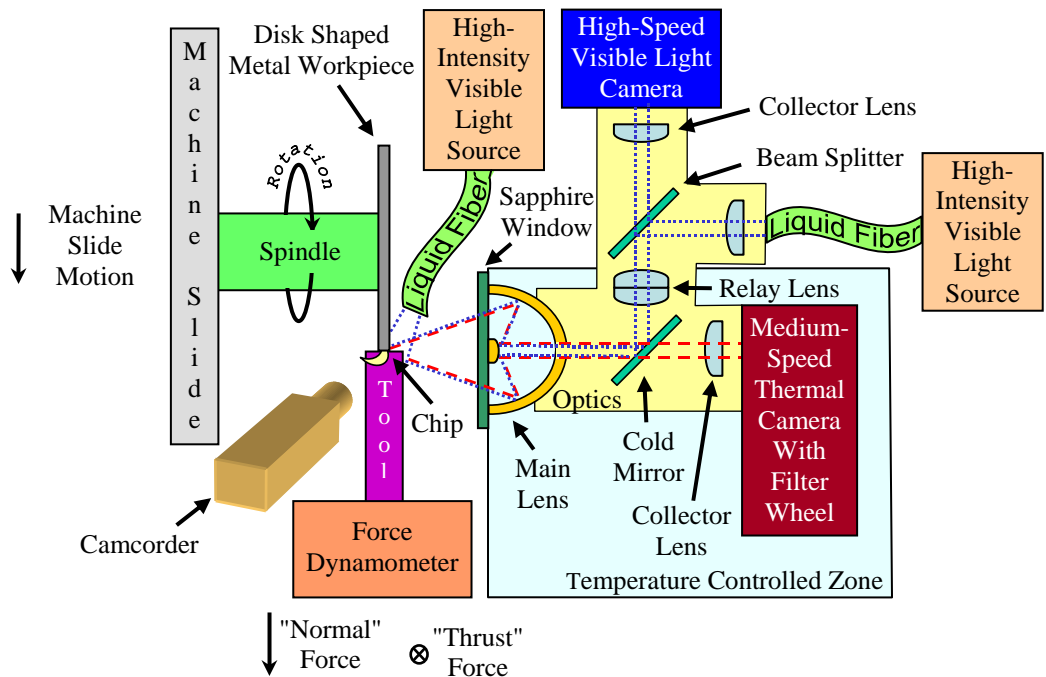
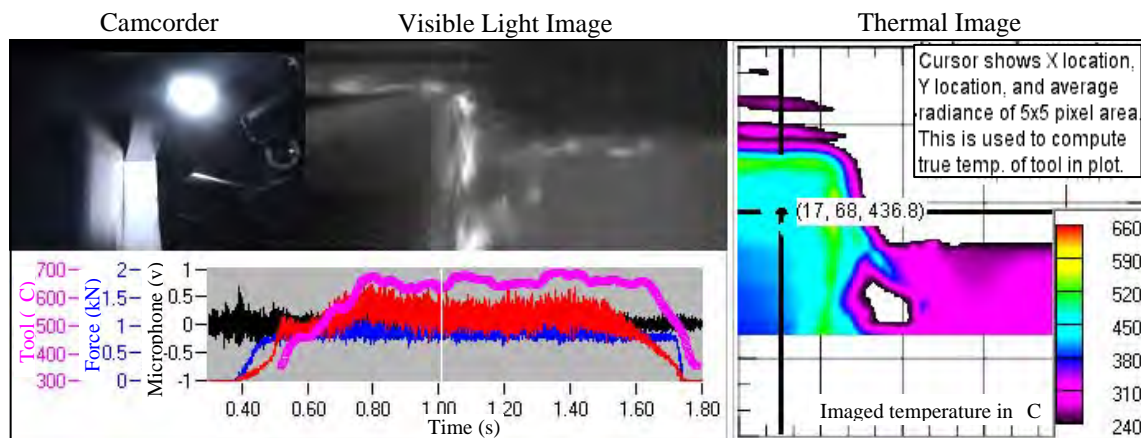


Fig. 2. The current dual-spectrum system.



Measured scalar data: true tool temperature (pink), cutting force (red), thrust force (blue), microphone signal (black)

Fig. 3. Typical synchronized dataset.

1.4 Recent work.

This paper presents two sets of results from recent work at NIST. The first addresses uncertainties in temperature measurements of small, rapidly moving features. The second addresses whether surface temperatures are an accurate measure of internal temperatures of the cutting tool.

TEMPERATURE MEASUREMENTS OF SMALL, RAPIDLY MOVING FEATURES

In real-world situations, multiple uncertainty sources often act together to affect a measured value. When imaging the metal cutting process, many features may range from $0.1 \mu\text{m}$ to $50 \mu\text{m}$ in size, such as the thickness of the shear zone. A variety of factors makes measuring the temperatures of such small features problematic. One factor is that spatial resolution is limited by the wavelength of light used to image the feature⁽⁸⁾. Visible light cameras are sensitive to wavelengths of less than $1 \mu\text{m}$, while thermal cameras are sensitive to wavelengths up to $24 \mu\text{m}$. This is the primary reason visible light cameras are generally able to image smaller features than thermal cameras. Also, if a feature is so small that it does not completely fill a pixel, the measured amplitude will be incorrect⁽⁸⁾. In addition, imperfections in the optics are more noticeable when imaging small features. One method for describing how the aforementioned effects influence the camera image is the *point spread function (PSF)*, which describes the response of an imaging system to a point source. It should be noted that diffraction effects^(8; 9) are also possible, but are ignored in this paper. *Motion blur* is the apparent streaking of rapidly moving objects.

Figure 4 shows a two dimensional model for the effects of the PSF and motion blur. The Appendix shows a Mathcad® implementation of the model. The undistorted, true intensity curve is modeled as a bar representing the shear zone of width W_{SZ} and height I_{SZ} , surrounded by a constant value I_{CF} representing the intensity of the chip face (term A of the convolution). This curve is convoluted with the normalized point spread function for the camera (term B) and a normalized bar of width W_{MB} representing the distance traveled by the shear zone during the integration time of the camera (term C). The area under both the point spread function (term B) and the motion blur curve (term C) is 1, so the area under the shear zone and chip face intensity curve (term A) is not altered by the convolution. However, the convolution will reduce the height and increase the width of the imaged shear zone.

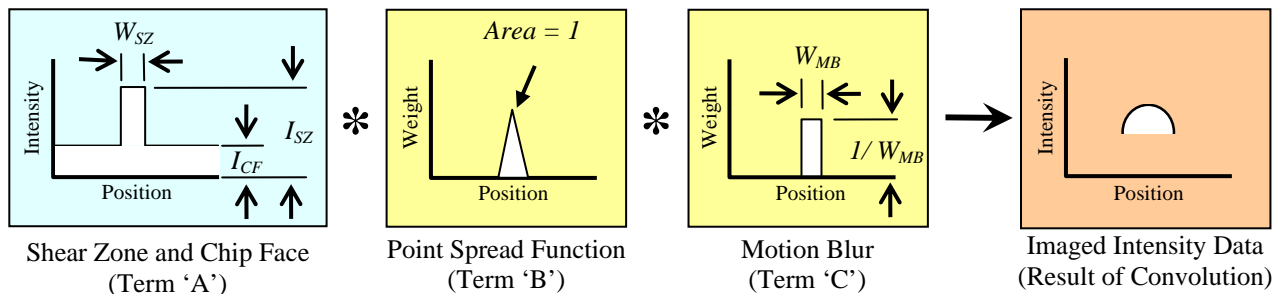


Fig. 4. Schematic of modeling measured intensity data as a convolution of several curves.

In theory, if one knows the PSF and W_{MB} , they may be deconvolved from the measured intensity data to compute the shear zone and chip face intensity curve. However, there are two difficulties with this approach. First, deconvolution is very sensitive to noise in the data. Computed results vary wildly in response to even small changes in the input data. Second, the imaged intensity data is often an incomplete data set. The reason that it may be an incomplete data set is that the chip face is often much cooler than the shear zone. In order to have enough sensitivity to measure the chip face temperature, the integration time must be increased. However, increasing the integration time also increases the motion blur. If the integration time is made too long, the motion blur can become so severe that the thermal image lacks sufficient detail. Thus, one often does not have data for the cooler portions of the measured intensity data.

An alternative approach is to select values for W_{SZ} , I_{SZ} , I_{CF} , W_{MB} , and the PSF. The convolution is computed and compared to the imaged intensity data. If there is good agreement, the selected values are plausible. One advantage to

this approach is that sensitivity analysis may be performed. For example, if changing I_{SZ} by a very large amount has little effect on how well the computed convolution matches the imaged data, the uncertainty in I_{SZ} is large. Figure 5 shows a data set of segmented titanium chip formation we will analyze using this approach. Note that the thermal image can not measure temperatures lower than 240 °C. The face of the chip is 240 °C or cooler while the shear zone is over 350 °C. To estimate W_{MB} (*MotionBlurWidth* in Appendix) successive visible light images were examined. To create an imaged intensity data set, a line through the shear zone was drawn in the thermal image. In addition to the data derived from Figure 5, the PSF for the camera (psp in Appendix), measured by the knife edge method, was used. The worksheet allows a user to input values for W_{SZ} (*ShearZoneWidth* in Appendix) and the temperature which corresponds to I_{CF} (*BaseLineTemperature* in Appendix). It then solves the convolution, setting the value of I_{SZ} (*ShearZoneIntensity* in Appendix) so that the area under the computed convolution curve is equal to the area under the imaged intensity curve. The **Root Mean Square (RMS)** value of the **residuals** (differences between imaged values and results of the convolution) is also generated.

To illustrate the importance of knowing W_{MB} , we will momentarily ignore the fact that we measured it using data from Figure 5. Figure 6 shows results where we assume $I_{CF} \cong 240$ °C and a range of W_{MB} and W_{SZ} are tried. The peak height of the imaged shear zone is shown as a horizontal line. Any valid value for T_{SZ} (the temperature corresponding to I_{SZ}) must be at or above this line. Notice that at each W_{SZ} , the values for T_{SZ} are nearly the same and seem like a single point in the plot, while the RMS value of the residuals are clearly different. Assume that when the RMS of the residuals is a minimum, the corresponding value of T_{SZ} is the most likely to be the correct value. Thus, when $W_{MB} = 41$ μm, $T_{SZ} \approx 660$ °C and when $W_{MB} = 16$ μm, $T_{SZ} \approx 370$ °C. Not knowing W_{MB} results in large uncertainty in our estimate of T_{SZ} .

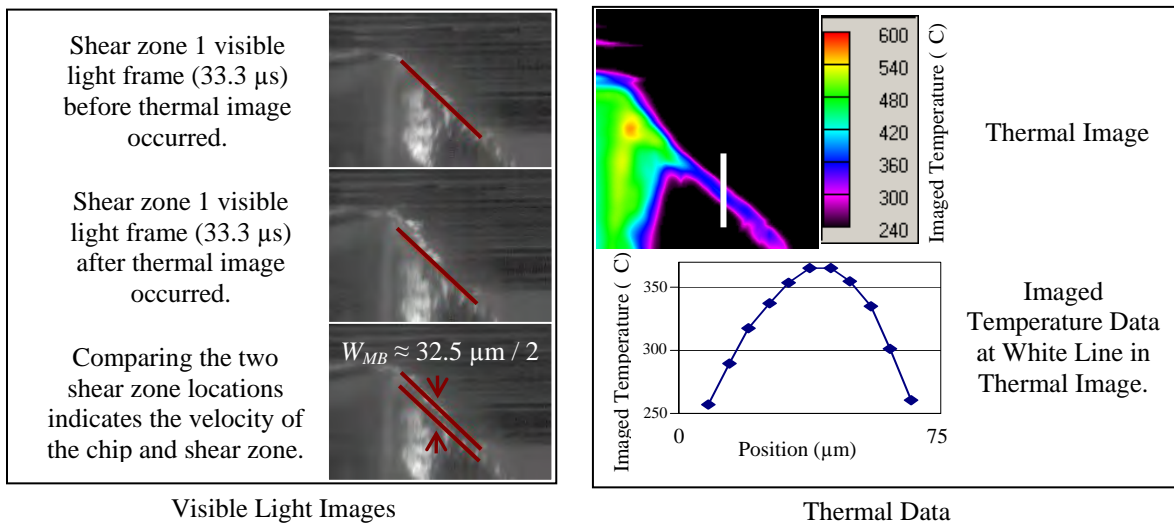


Fig. 5. Visible and thermal spectrum images used to estimate W_{MB} and imaged intensity data.

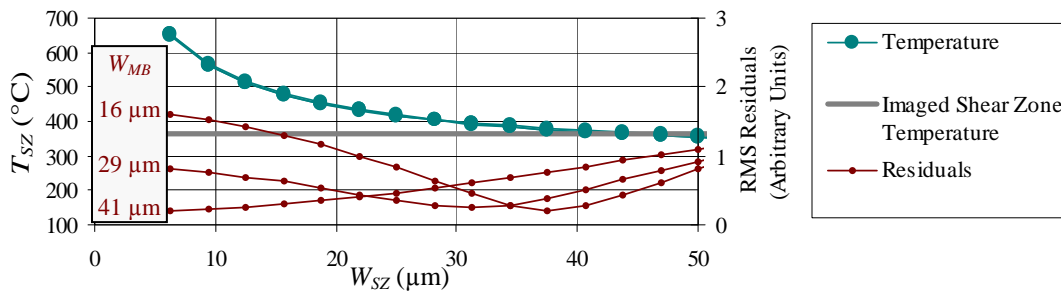


Fig. 6. Results where $I_{CF} \cong 240$ °C and W_{MB} is assumed to be unknown.

It is interesting to note that the primary factor determining whether the computed convolution is a good fit to the measured image intensity (the RMS of the differences is small) is how well the widths of the two curves match. This is illustrated by the example shown in Figure 7.

In Figure 8, we take advantage of our measured value for W_{MB} . Figure 8b shows the same data as Figure 8a, but zoomed in on the portion most relevant to the discussion below. Three values for W_{MB} are tried, 10 μm , 16.25 μm , and 22.5 μm . These values correspond to the value for W_{MB} measured in Figure 5, as well as +1 thermal image pixel and -1 thermal image pixel. It is assumed that we have measured W_{MB} to this level of accuracy. We assume I_{CF} corresponds to either 240 $^{\circ}\text{C}$ or 130 $^{\circ}\text{C}$. $I_{CF} \cong 20^{\circ}\text{C}$ was also tried and yielded results similar to 130 $^{\circ}\text{C}$, so results for 20 $^{\circ}\text{C}$ are not shown. The range of likely T_{SZ} is shown in the two gold colored ovals in Figure 8b. We can safely say that T_{SZ} (the apparent temperature of the shear zone) is between 366 $^{\circ}\text{C}$ and 384 $^{\circ}\text{C}$. Emissivity may be determined after the cutting test⁽¹⁰⁾ and used to convert this into a range of plausible true temperatures for the shear zone.

Note that if $I_{CF} \cong 240^{\circ}\text{C}$, the narrower (34 μm to 41 μm), hotter (368 $^{\circ}\text{C}$ to 384 $^{\circ}\text{C}$) shear zone values are more likely to be correct. If $I_{CF} \cong 130^{\circ}\text{C}$, the wider (50 μm), cooler (366 $^{\circ}\text{C}$ to 368 $^{\circ}\text{C}$) shear zone values are more likely. Knowing the chip face temperature is important information – even if the shear zone temperature is the ultimate goal. A repeat test, with the same cutting conditions but a long enough integration time to capture the chip face temperature, may be useful here. This data indicates that motion blur and PSF effects may be more accurately compensated for if other information, such as chip face temperature, is measured.

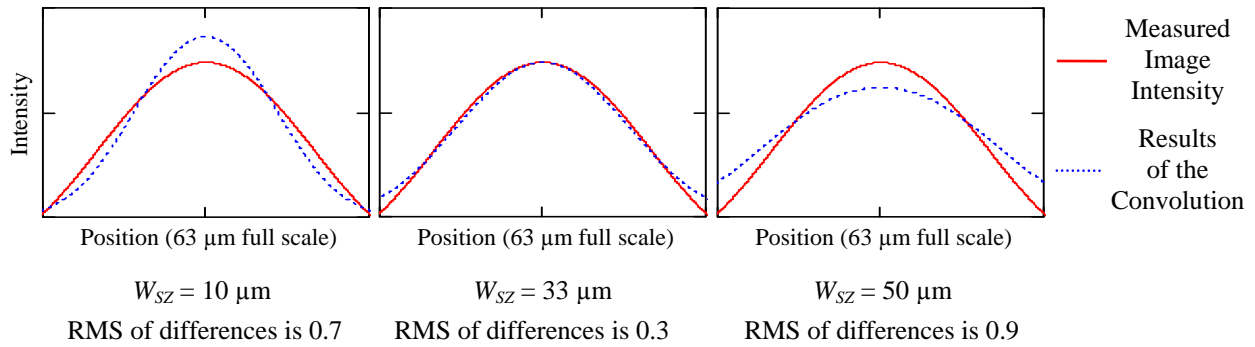


Fig. 7. Illustrative example showing that the lowest RMS of the differences is obtained when the width of the measured image intensity curve matches the width of the resulting convolution. $I_{CF} \cong 240^{\circ}\text{C}$ and $W_{MB} = 29 \mu\text{m}$.

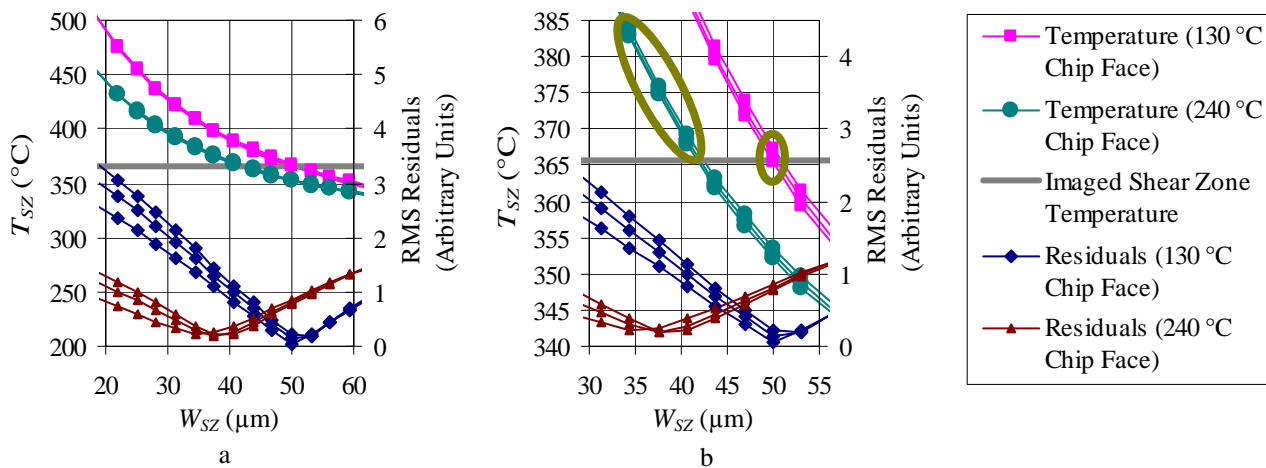


Fig. 8. Results where I_{CF} is assumed to correspond to either 130 $^{\circ}\text{C}$ or 240 $^{\circ}\text{C}$, and W_{MB} is the measured value, the measured value + 1 thermal image pixel, and the measured value - 1 thermal image pixel.

DOES SURFACE TEMPERATURE REVEAL INTERNAL TEMPERATURE?

Thermal imaging indicates the temperature on the surface of an object. Researchers typically assume that the surface temperature is indicative of the temperature inside the object. This section presents an attempt to verify this assumption for a cutting tool. First, grooves were cut into a tool, as shown in Figure 9. Thermocouples were then cemented into the grooves with high temperature cement. The cement was selected to have a thermal conductivity and thermal expansion similar to that of the cutting tool. The temperature sensitive portions of the thermocouples were positioned so that they are approximately where the center of the chips will be during machining. It should be noted that the grooves significantly weakened the tool. Thus, aggressive cutting conditions can not be used with this tool.

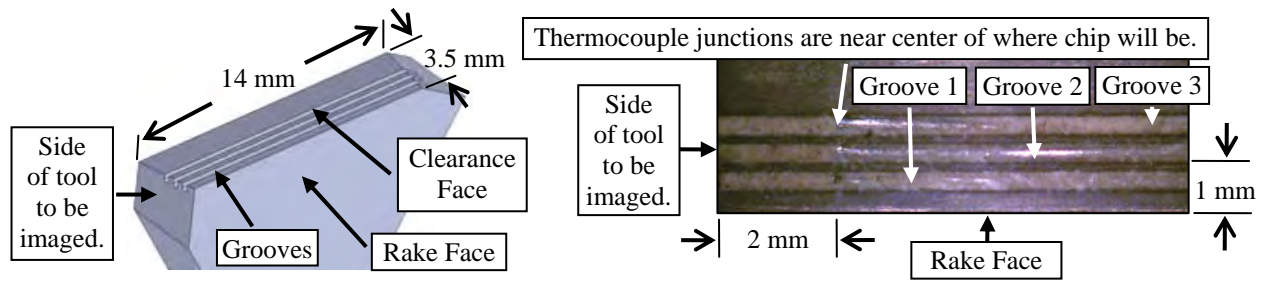


Fig. 9. Isometric view (drawing on left) and top view (photo on right) of grooves in the cutting tool.

Figure 10 shows the instrumented tool temporarily wrapped in aluminum foil and heated by thermal tweezers. A thermal image is acquired after 10 minutes. This serves several purposes. First, water in the cement is driven off. Second, an oxide layer is formed on the tool and the cement, preventing changes in emissivity during the cutting experiments. Finally, comparing the thermal image to the true temperature of the tool allows the emissivity of the cement in the grooves to be measured.

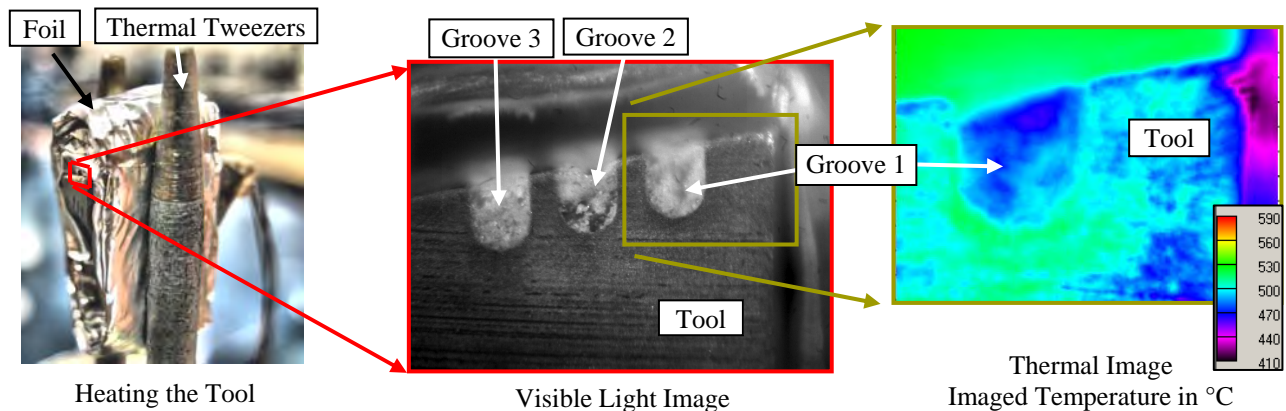


Fig. 10. Heating instrumented cutting tool in thermal tweezers.

The instrumented tool is then mounted and a cutting experiment performed with a 3.2 mm wide steel workpiece. Only Groove 1 is imaged in this experiment. Groove 2 and Groove 3 are used in a different experiment. In contrast to the chip, the tool is stationary in the images, and the surface is relatively uniform. Also, we are only concerned with an average temperature in the relatively large area of the cement filled groove. Therefore, there is no need to correct for the PSF of the camera or for motion blur in the images.

Figure 11 shows the resulting true temperature of the cement reported by the thermal camera, as well as the thermocouple temperature. There is good agreement during some portions of the test and less agreement during other portions. There are several possible explanations for this behavior which are currently being explored. This data indicates that a thermal camera measurement of the side of the cutting tool is representative of temperature within the tool, at least during steady-state cutting.

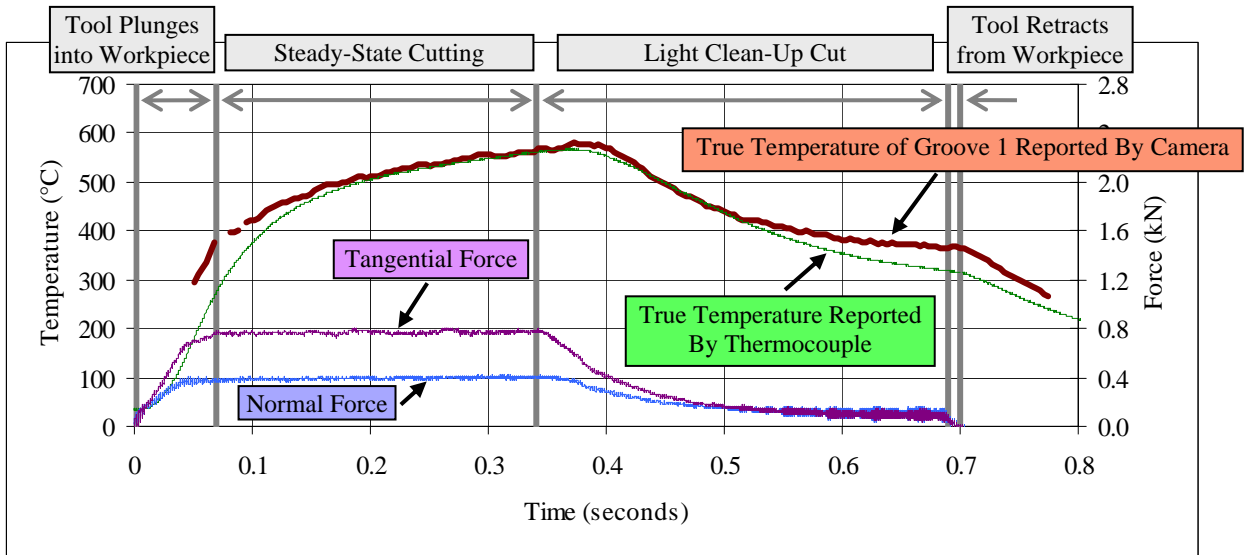


Fig. 11. Comparing thermocouple and camera temperatures. Cutting forces indicate when cutting at the full depth of cut occurred (between about 0.07 s and 0.34 s). Cutting between 0.34 s and 0.69 s is a light cut which insures the disk is circular for the next test.

CONCLUSIONS

Dual-spectrum imaging is a powerful technique for enabling a better understanding of the metal cutting process. However, uncertainty sources need to be understood to correctly acquire and interpret the data. Two recent results were presented. The first indicates that motion blur and PSF effects can cause significant uncertainties in the estimated temperatures of small features, such as the shear zone. These uncertainties may be compensated for if other information, such as chip face temperature, is measured. The second indicates that a thermal camera measurement of the side of the cutting tool is representative of temperature within the tool, at least during steady-state cutting.

ACKNOWLEDGEMENTS

The authors wish to acknowledge Robert Ivester, Johannes Soons, and Howard Yoon of the National Institute of Standards and Technology.

REFERENCES

- [1] Ivester, R. W. and Heigel, J. C., "Smart Machining Systems: Robust Optimization and Adaptive Control Optimization for Turning Operations," *Transactions of the North American Research Institute (NAMRI)/SME*, Vol. 35, 2007, pp. 505-511.
- [2] Whintenton, E. P., Ivester, R. W., and Yoon, H., "Simultaneous Visible And Thermal Imaging Of Metals During Machining," *SPIE Proceedings*, Vol. 5782, 2005, pp. 71-82.
- [3] Heigel, J. C., Ivester, R. W., and Whintenton, E. P., "Cutting Temperature Measurements of Segmented Chips using Dual-Spectrum High-Speed Microvideography," *Transactions of the North American Research Institute (NAMRI)/SME*, Vol. 36, 2008, pp. 73-80.
- [4] Whintenton, E. P., Heigel, J. C., and Ivester, R. W., "Measurement and Characterization of Dynamics in Machining Chip Segmentation," *11th CIRP International Workshop on Modeling of Machining Operations*, 2008, pp. 237-246.
- [5] Ivester, R. W., Whintenton, E. P., Heigel, J. C., Marusich, T., and Arthur, C., "Measuring Chip Segmentation by High-Speed Microvideography and Comparison to Finite-Element Modeling Simulations," *10th CIRP International Workshop on Modeling of Machining Operations*, 2007, pp. 37-44.
- [6] Gnanamanickam, E., Huang, C., Murthy, T. G., Sullivan, J. P., and Chandrasekar, S., "In Situ Measurement of Deformation and Temperature in Machining," *12th CIRP Conference on Modelling of Machining Operations*, 2009, pp. 384-388.
- [7] Heigel, J. C. and Whintenton, E. P., "High-Speed Microvideography Observations of the Periodic Catastrophic Shear Event in Cutting AISI 1045 Steel," *Transactions of the North American Research Institute (NAMRI)/SME*, Vol. 37, 2009, pp. 33-40.
- [8] Holst, G. C., *Holst's Practical Guide to Electro-Optical Systems*, JCD Publishing 2003.
- [9] Shirley, E. L., "Revised Formulas for Diffraction Effects with Point and Extended Sources," *Applied Optics*, Vol. 37, No. 28, 1998, pp. 6581-6590.
- [10] Whintenton, E. P., "Characterization of Uncertainties When Measuring Metal Cutting Temperatures Using Infrared Radiation Thermography," *SPIE Proceedings*, Vol. 7299, 2009, pp. 72990G-8.

APPENDIX - MATHCAD® DOCUMENT TO ANALYSE SHEAR ZONE TEMPERATURE MEASUREMENTS.

This software was developed at the National Institute of Standards and Technology by employees of the Federal Government in the course of their official duties. Pursuant to title 17 Section 105 of the United States Code this software is not subject to copyright protection and is in the public domain. This is an experimental system. NIST assumes no responsibility whatsoever for its use by other parties, and makes no guarantees, expressed or implied, about its quality, reliability, or any other characteristic. We would appreciate acknowledgement if the software is used.

Correcting for Motion Blur and PSF in Thermal Measurement of a Shear Band
Eric Whitenon
NIST

Note that some variables are defined globally at the bottom of this document !

Second radiation constant - $c2 := 14387.67$

Offset to convert degrees C to degrees K - $koff := 273.15$

Mathcad tolerance constants - $TOL := 10^{-99}$ $CTOL := 10^{-99}$

Range of lambda, in micrometers, the camera is sensitive to - $\lambda1 := 3.80$ $\lambda2 := 5.10$

Values will be integrated over the range of lambda using simpsons rule - $n\lambda := 1001$ $i := 0..n\lambda - 1$ $\lambda_i := \lambda1 + \frac{(\lambda2 - \lambda1) \cdot i}{n\lambda - 1}$

Temperature values in degrees C -

$T :=$  $nT := \text{rows}(T)$ $j := 0..nT - 1$
C...\thermal-data.txt

Compute unitless intensity data with baseline removed -

$$I_j := \frac{\sum_i \frac{1}{|\lambda_i|^5 \cdot \left[e^{\frac{c2}{\lambda_i(T_j+koff)}} - 1 \right]}}{n\lambda}$$

$$\text{BaseLineIntensity} := \frac{\sum_i \frac{1}{|\lambda_i|^5 \cdot \left[e^{\frac{c2}{\lambda_i(\text{BaseLineTemperature}+koff)}} - 1 \right]}}{n\lambda}$$

$$I_j := I_j - \text{BaseLineIntensity}$$

Model intensity data as Sinc Function. This will not work for some data sets. There are several reasons to model intensity as a Sinc Function. The primary reason is that it facilitates alignment (in X) of the intensity data to the results of the convolution.

Estimate parameters for Sinc Function fit of intensity data -

$$\text{PeakHeight} := \max(I)$$

$$\text{PeakCenter} := \frac{\sum_j |I_j \cdot j|}{\sum_j |I_j|}$$

$$\text{PeakWidth} := \frac{\sum_j |I_j \cdot |j - \text{PeakCenter}||}{2 \cdot \pi \cdot \sum_j |I_j|}$$

Perform fit of Sinc Function to intensity data -

$$X_j := j \quad G := \begin{pmatrix} \text{PeakHeight} \\ \text{PeakCenter} \\ \text{PeakWidth} \end{pmatrix} \quad F(x, a, b, c) := a \cdot \text{sinc}[c \cdot (x - b)] \quad G := \text{genfit}(X, I, G, F)$$

$$\text{PeakHeight} := G_0 \quad \text{PeakCenter} := G_1 \quad \text{PeakWidth} := G_2$$

Resample (and extend and center) data - $Nk := \text{ResScale} \cdot nT \cdot \text{ResExt}$ $k := 0..Nk - 1$ $\text{ResOff} := \text{floor}\left(\frac{Nk}{2}\right)$

Resample intensity data - $\text{ResIFit}_k := F\left[\left(\frac{k - \text{ResOff}}{\text{ResScale}}\right), \text{PeakHeight}, 0, \text{PeakWidth}\right]$ $\text{SumSqResIFit} := \sum_k |\text{ResIFit}_k|^2$

Get camera point spread function (right half of) from disk file. Goes from 1 to 0 -

For convenience, the PSF is centered in the data set while the other convolution terms are centered around time 0

$$\begin{aligned}
 & \text{psp} := \text{get_file}(\text{C:\D...\psp.txt}) \quad nP := \text{rows}(\text{psp}) \quad p := 0..nP - 1 \\
 & \text{vx}_p := p \quad \text{vs} := \text{lspline}(\text{vx}, \text{psp}) \\
 & \text{fTemp}(kk) := \begin{cases} 0 & \text{if } kk > nP \\ \text{interp}(\text{vs}, \text{vx}, \text{psp}, kk) & \text{otherwise} \end{cases} \quad \text{ResPSF}_k := \text{fTemp}\left(\frac{k - \text{ResOff}}{\text{ResScale}}\right)
 \end{aligned}$$

Normalize point spread function of camera -

$$\text{Temp} := \sum_k \text{ResPSF}_k \quad \text{ResPSF}_k := \frac{\text{ResPSF}_k}{\text{Temp}}$$

Normalized motion blur bar -

$$\text{fTemp}(kk) := \begin{cases} 1 & \text{if } kk < \frac{\text{MotionBlurWidth}}{2} \\ 1 & \text{if } \frac{Nk}{\text{ResScale}} - kk < \frac{\text{MotionBlurWidth}}{2} \\ 0 & \text{otherwise} \end{cases} \quad \text{ResMotionBlur}_k := \text{fTemp}\left(\frac{k}{\text{ResScale}}\right)$$

$$\text{Temp} := \sum_k \text{ResMotionBlur}_k \quad \text{ResMotionBlur}_k := \frac{\text{ResMotionBlur}_k}{\text{Temp}}$$

Convolve fit of measured data with shear zone "bar" of unit height with motion blur and camera response to determine intensity of shear zone bar -

$$\text{Factors to correct for the way Mathcad scales the cfft and icfft functions -} \quad \text{cfftScale} := \sqrt{Nk} \quad \text{icfftScale} := \frac{1}{\sqrt{Nk}}$$

Width in pixels of shear zone -

$$\text{fTemp}(kk) := \begin{cases} 1 & \text{if } kk < \frac{\text{ShearZoneWidth}}{2} \\ 1 & \text{if } \frac{Nk}{\text{ResScale}} - kk < \frac{\text{ShearZoneWidth}}{2} \\ 0 & \text{otherwise} \end{cases} \quad \text{ResShearZone}_k := \text{fTemp}\left(\frac{k}{\text{ResScale}}\right)$$

Convolve -

$$\begin{aligned}
 T1 & := \text{cfftScale} \cdot \text{cfft}(\text{ResPSF}) & T2 & := \text{cfftScale} \cdot \text{cfft}(\text{ResMotionBlur}) & T3 & := \text{cfftScale} \cdot \text{cfft}(\text{ResShearZone}) \\
 T4_k & := T1_k \cdot T2_k \cdot T3_k & \text{ResConvolved} & := \text{icfftScale} \cdot \text{icfft}(T4)
 \end{aligned}$$

Re-generate shear zone bar at correct amplitude-

$$\text{Temp} := \frac{\sum_{k = \text{ResOff} - \frac{Nk}{2\text{ResExt}}}^{\text{ResOff} + \frac{Nk}{2\text{ResExt}}} |\text{ResFit}_k|}{\sum_{k = \text{ResOff} - \frac{Nk}{2\text{ResExt}}}^{\text{ResOff} + \frac{Nk}{2\text{ResExt}}} |\text{ResConvolved}_k|} \quad \text{ResShearZone}_k := \text{Temp} \cdot \text{ResShearZone}_k$$

Recompute convolution -

$$T3 := \text{cffScale} \cdot \text{cff}(\text{ResShearZone})$$

$$T4_k := T1_k \cdot T2_k \cdot T3_k$$

$$\text{ResIConvolved} := \text{icfftScale} \cdot \text{icfft}(T4)$$

Add baseline intensity back in -

$$\text{ShearZoneIntensity} := \max(\text{ResShearZone}) + \text{BaseLineIntensity}$$

$$\text{ResIFit} := \text{ResIFit} + \text{BaseLineIntensity}$$

$$\text{ResIConvolved} := \text{ResIConvolved} + \text{BaseLineIntensity}$$

Determine residuals in area of original (non-extended) data-

$$\text{residuals} := \frac{\sum_{k = \text{ResOff} - \frac{Nk}{2\text{ResExt}}}^{\text{ResOff} + \frac{Nk}{2\text{ResExt}}} |\text{ResIFit}_k - \text{ResIConvolved}_k|^2}{\frac{Nk}{\text{ResExt}}}$$

Determine shear zone temperature -

Use maximum temperature measured as initial guess -

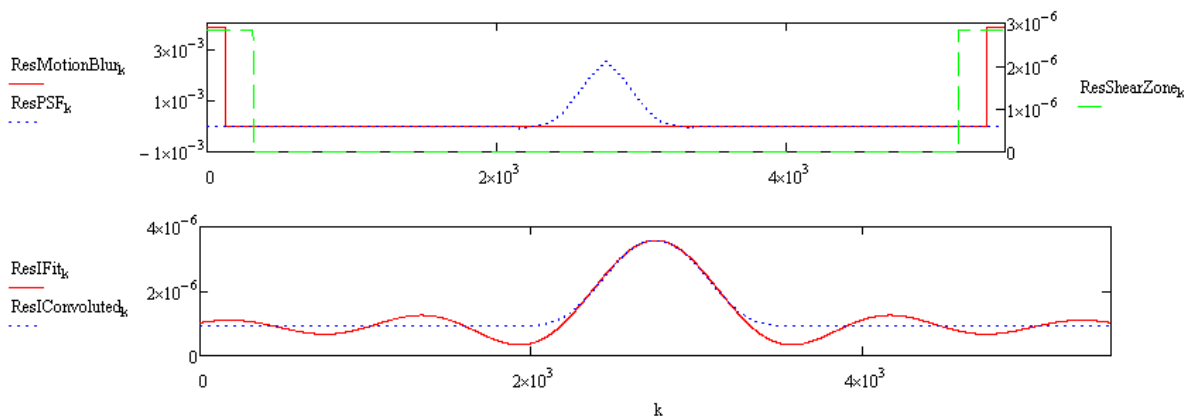
$$\text{MaxTemperatureMeasured} := \max(T)$$

given

$$Q(\text{ttt}) := \text{ShearZoneIntensity} - \frac{\sum_i \frac{1}{|\lambda_i|^5 \cdot \left[e^{\frac{c2}{\lambda_i(\text{ttt} + \text{koff})}} - 1 \right]}}{n\lambda}$$

$$\text{ShearZoneTemperature} := \text{Minimize}(Q, \text{MaxTemperatureMeasured})$$

RESULTS



INPUTS		OUTPUTS	
Baseline temperature in degrees C -	BaseLineTemperature = 230	Fit error in arb units -	residuals = 1.556 × 10 ⁻⁹
Shear zone width in pixels -	ShearZoneWidth = 6.5	Max temperature measured degrees C -	MaxTemperatureMeasured = 365.7
Width in pixels of blur due to motion-	MotionBlurWidth = 2.6	Shear zone temperature in degrees C -	ShearZoneTemperature = 371.413
Rescale # data points, more accuracy -	ResScale = 100		
Extend data set so all of function included-	ResExt = 5		